Species-resolved, single-cell respiration rates reveal dominance of sulfate reduction in a deep continental subsurface ecosystem

Melody R. Lindsay[a,1], Timothy D'Angelo[a], Jacob H. Munson-McGee[a], Alireza Saidi-Mehrabad[b], Molly Devlin[b,c], Julia McGonigle[a], Elizabeth Goodell[a,d], Melissa Herring[a,e], Laura C. Lubelczyk[a], Corianna Mascena[a], Julia M. Brown[a], Greg Gavelis[a], Jiarui Liu[f], D. J. Yousavich[f], Scott D. Hamilton-Brehm[g], Brian P. Hedlund[c], Susan Lang[h], Tina Treude[f,i], Nicole J. Poulton[a], Ramunas Stepanauskas[a], Duane P. Moser[b], David Emerson[a], and Beth N. Orcutt[a]

Rates of microbial processes are fundamental to understanding the significance of microbial impacts on environmental chemical cycling. However, it is often difficult to quantify rates or to link processes to specific taxa or individual cells, especially in environments where there are few cultured representatives with known physiology. Here, we describe the use of the redox-enzyme-sensitive molecular probe RedoxSensor™ Green to measure rates of anaerobic electron transfer physiology (i.e., sulfate reduction and methanogenesis) in individual cells and link those measurements to genomic sequencing of the same single cells. We used this method to investigate microbial activity in hot, anoxic, low-biomass ($\sim 10^3$ cells mL^{-1}) groundwater of the Death Valley Regional Flow System, California. Combining this method with electron donor amendment experiments and metatranscriptomics confirmed that the abundant spore formers including *Candidatus* Desulforudis audaxviator were actively reducing sulfate in this environment, most likely with acetate and hydrogen as electron donors. Using this approach, we measured environmental sulfate reduction rates at 0.14 to 26.9 fmol cell^{-1} h^{-1}. Scaled to volume, this equates to a bulk environmental rate of $\sim 10^3$ pmol sulfate L^{-1} d^{-1}, similar to potential rates determined with radiotracer methods. Despite methane in the system, there was no evidence for active microbial methanogenesis at the time of sampling. Overall, this method is a powerful tool for estimating species-resolved, single-cell rates of anaerobic metabolism in low-biomass environments while simultaneously linking genomes to phenomes at the single-cell level. We reveal active elemental cycling conducted by several species, with a large portion attributable to *Ca.* Desulforudis audaxviator.

deep biosphere | sulfate reduction | single-cell genomics | RedoxSensor Green | carbon monoxide

Measurements of metabolic rates of microorganisms in their natural environment are necessary for understanding biogeochemical cycling on both local and global scales. The deep subsurface is immense and hosts a substantial fraction of all bacterial and archaeal cells (1–3), yet is one of the least understood biotic environments on Earth. Due to the proliferation of subsurface microorganisms under extreme energy limitation and relative isolation from the photosphere (4), deep subsurface microorganisms also serve as important models in the search for life on other planets (5–7). Known primary energy metabolisms in anoxic subsurface habitats include sulfate reduction, methanogenesis, hydrogenotrophy, carboxydotrophy, and various types of fermentation (8–10). However, the quantification of these processes in the subsurface is difficult, due to exceptionally low biomass (11), low thermodynamic yields (12), and difficulty in obtaining quality samples. Currently, there are only a handful of subsurface environments on Earth where microbial sulfate reduction rates have been quantified at the bulk scale, with values ranging from tens to thousands of nanomoles of sulfate reduced per liter per day (13–15). These measurements required long incubation times (i.e., days to weeks) with radiotracer amendments, resulting in potential bulk rates of activity that must be cautiously interpreted as proxies for in situ rates. Moreover, bulk rates fail to account for the immense genomic and phenotypic diversity among subsurface microbial cells (16, 17). Recently, subsurface ecosystems in terrestrial, deep (>500 m below land surface) samples collected through drilled wells or mine boreholes evaluated with -omics tools including metagenomics, metatranscriptomics, and single-cell genomics (18, 19) have shown that sulfate-reducing species such as *Candidatus* Desulforudis audaxviator of the phylum Firmicutes (*Bacillota*) (20) and methanogenic archaea often dominate (3, 9, 21). However, studies evaluating in situ microbial activities in the subsurface are limited (10, 22) and cell-specific rates remain largely unknown. A grand challenge, then, is to ascribe quantifiable activity to individual cells in situ and link this information with corresponding genomes, which requires the use of

Significance

Microbial life is essential for the functioning of ecosystems, yet we often do not know which microbes are responsible for which processes and the speed at which they cycle elements. We developed a proxy to estimate element turnover rates for two critical microbial processes—sulfate reduction and biogenic methane production—that also links these physiologies to specific microbial cells. When applied to a deep fractured rock ecosystem, where current methods for detecting microbial activity would be difficult, we showed this approach to be a powerful tool to measure microbial activity and to link activity to individual cells. Moreover, we resolved single-cell rates of sulfate reduction in a deep subsurface environment, which has not been possible before.

functional genomic analyses that target metabolisms predicted by environmental genomics.

A new method for integrated single-cell genome and phenome analyses was recently described for microbial oxygen respiration (17). This approach harnesses the molecular probe RedoxSensor™ Green (RSG; Invitrogen). The fluorescence intensity of RSG correlates with the respiratory rate of individual cells and can be measured in the same cells that are sorted by fluorescence-activated cell sorting (FACS) for single-cell genome sequencing. As an added benefit, this method requires only short incubations and minimal sample volumes, thus facilitating studies of low-biomass and low-energy environments and minimizing "bottle effects" (23) inherent to longer incubations. Since the fluorescent RSG signal is based on electron transfer (24) carried out by a broad class of oxidoreductase enzymes, we hypothesized that its use may not be limited to aerobic respiration and could also be applied to any metabolism that involves electron transfer to RSG. Here, we describe an RSG-based method to measure rates, at single-cell resolution, for two critical anaerobic processes—dissimilatory sulfate reduction and methanogenesis. We applied this method to freshly collected samples from 750 meters below land surface (mbls) at Inyo-BLM 1, a borehole which accesses hot (57 °C), paleometeoric fracture water of the Death Valley Regional Flow System (DVRFS) (19, 25–27). We coupled our RSG-derived rate measurements with single-cell genomics, metatranscriptomics, and bulk rate measurements using radiotracers.

This study aimed to test the hypothesis that abundant species in anoxic fluids of Inyo-BLM 1, including the endospore former *Ca.* Desulforudis audaxviator, are actively respiring sulfate in situ and that their activity may be stimulated by electron donor addition. *Ca.* Desulforudis audaxviator has previously been shown to represent a large proportion of low-biomass, low-energy, subsurface aquifer systems (18, 19, 21), but until now species- and cell-specific respiration rates of key energy-conserving processes (i.e., sulfate reduction) have not been confirmed in situ and linked directly to these cells. To test our hypotheses, we incubated borehole fluids with amendments of acetate, hydrogen, and carbon monoxide and analyzed incubated and unmanipulated fluids with our RSG-labeling approach, coupled to FACS and single-cell genome sequencing. This was complemented by metatranscriptomics and radiotracer bulk rate measurements. Our results demonstrate that *Ca.* Desulforudis audaxviator and most other abundant cells are active in the deep subsurface and highlight the potential of this methodological approach to identify active microbial cells in environments where it is difficult to obtain large amounts of sample or to measure respiration rates.

Results and Discussion

Anaerobic Respiration Rates Can Be Determined with an RSG-Based Proxy. RSG has been used in previous studies as a qualitative indicator of cell viability or respiratory activity (24, 28, 29) and with seawater samples to quantify aerobic respiration rates of marine prokaryoplankton (17). However, to our knowledge, cell-specific rates of anaerobic respiration rates have not been reported. To determine whether the RSG-based proxy could be extended to study anaerobic respiration, we analyzed the relationship between RSG fluorescence measured with a ZE5 flow cytometer and the rates of sulfate reduction (Fig. 1*A*) and methanogenesis (Fig. 1*B*) in a variety of stationary-phase pure cultures following a similar, recently described approach that was used to study aerobic respiration (17) (*Materials and Methods* and Dataset S1). These particular metabolic processes were targeted because of the dominance of sulfate reducers and methanogens in many terrestrial deep-subsurface ecosystems (21, 30). Our culture experiments yielded positive relationships between RSG fluorescence and the rate of production of sulfide by phylogenetically distinct sulfate-reducing microbial cultures ($R^2 = 0.95$), and the rate of methane produced from both acetoclastic and hydrogenotrophic methanogen cultures ($R^2 = 0.66$) according to the equations fully described in the *Materials and Methods*. Given uncertainty about
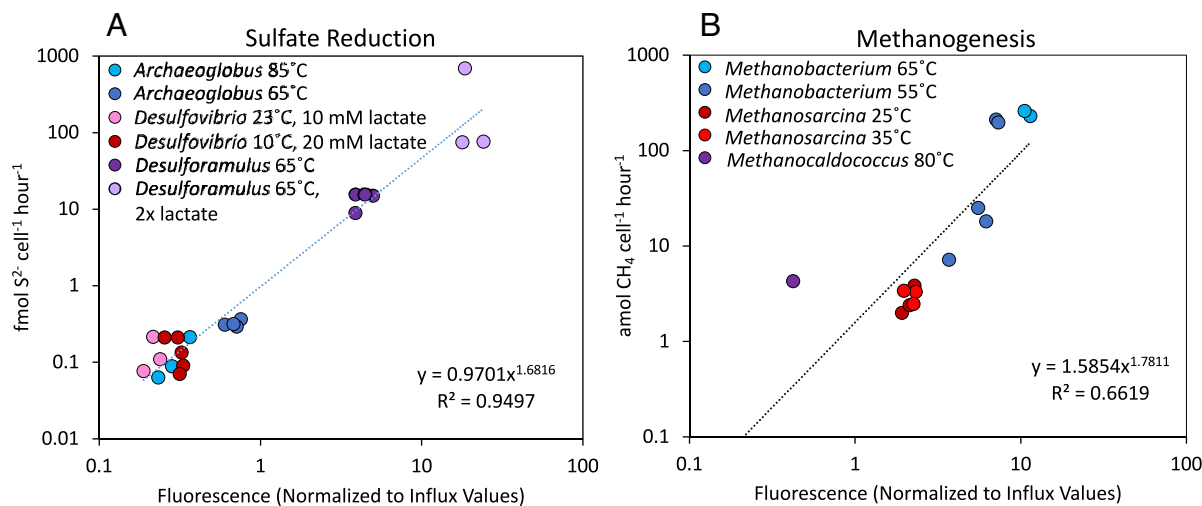

Fig. 1. Calibration of RSG-based proxy for sulfate reduction and methanogenesis. (*A*) Comparison of normalized RSG fluorescence intensity against cell-specific sulfide production/sulfate reduction rates in laboratory cultures. Each data point represents one experiment with a different sulfate reducer under defined culture conditions, including the species *A. fulgidus* at 85 °C and 65 °C, *Desulfovibrio vulgaris* at 23 °C & 10 mM lactate and 10 °C & 20 mM lactate, and *D. putei* at 65 °C (isolated from Inyo-BLM 1; more information on cultures and experimental conditions in Dataset S1). A comparison of this figure with one high rate value outlier point removed is depicted in *SI Appendix*, Fig. S1. (*B*) Comparison of normalized RSG fluorescence intensity against cell-specific methanogenesis rates in laboratory cultures. Each data point represents one experiment with a different methanogenic archaeon, including a *Methanobacterium* enriched from Inyo-BLM 1 at 65 °C and 55 °C, *M. barkeri* at 25 °C and 35 °C, and *Methanocaldococcus jannaschii* at 80 °C. For both comparisons, all fluorescence values were measured on a ZE5 Cell Analyzer flow cytometer but were normalized to fluorescence bead standards used to calibrate the flow cytometers in order to display values comparable to fluorescence measurements from the BD InFlux Mariner flow cytometer (see normalization procedure in *Materials and Methods*). Growth curve proxies based on sulfide concentrations (for sulfate reducers) or methane concentrations (for methanogens) and cell counts are provided in *SI Appendix*, Figs. S2 and S3, respectively. Representative flow cytometry gates for each culture species are depicted in *SI Appendix*, Figs. S11 and S12.

the electron-transfer mechanisms by which RSG can be reduced (28), potential quantitative relationships between RSG fluorescence and metabolic rates could be further explored with other anaerobic metabolisms. Further calibrations and benchmarking could allow for the exploration of other anoxic ecosystems.

Within the cultures used for the RSG calibration, sulfide production ranged from 0.063 to 688 fmol sulfide cell^{-1} h^{-1}, (while one experiment exhibited an extremely high production value of 688 fmol sulfide cell^{-1} h^{-1}, the next highest value was 76 fmol sulfide cell^{-1} h^{-1}), and methane production ranged from 1.97 to 258 amol methane cell^{-1} h^{-1}, with the lower value for each process being the lower limit of quantification for our culture calibration RSG rate calculations. There was one outlier sulfate reduction rate datum which minimally affected results depicted in Fig. 1 (culture calibration), and therefore calculated rates of cell-specific sulfate reduction. For comparison purposes, rate results calculated without this one outlier data

point are presented in *SI Appendix,* Fig. S1. Additional experiments with the cultures of the sulfate reducer *Desulforamulus* (basonym: *Desulfotomaculum*) *putei* that was originally obtained from Inyo-BLM 1 subsurface fluids (described in *Materials and Methods*) were done in both exponential and stationary growth phases to assess effects of growth phase on RSG fluorescence. These cultures grew to a relatively low density compared with the other cultures (*SI Appendix,* Fig. S2) but exhibited some of the highest per-cell rates of sulfate reduction measured in cultures compared with previously published rates of psychrophilic or mesophilic cultures (Fig. 1*A*) (31). These high rates could be because these are environmental thermophiles that were isolated from a nutrient-poor environment and given an abundance of carbon sources (*Materials and Methods*), which would allow them to potentially metabolize a larger amount of substrate in a shorter period of time. We detected a stronger relationship between RSG fluorescence and activity for stationary-phase cultures (*SI Appendix,* Fig. S4), which
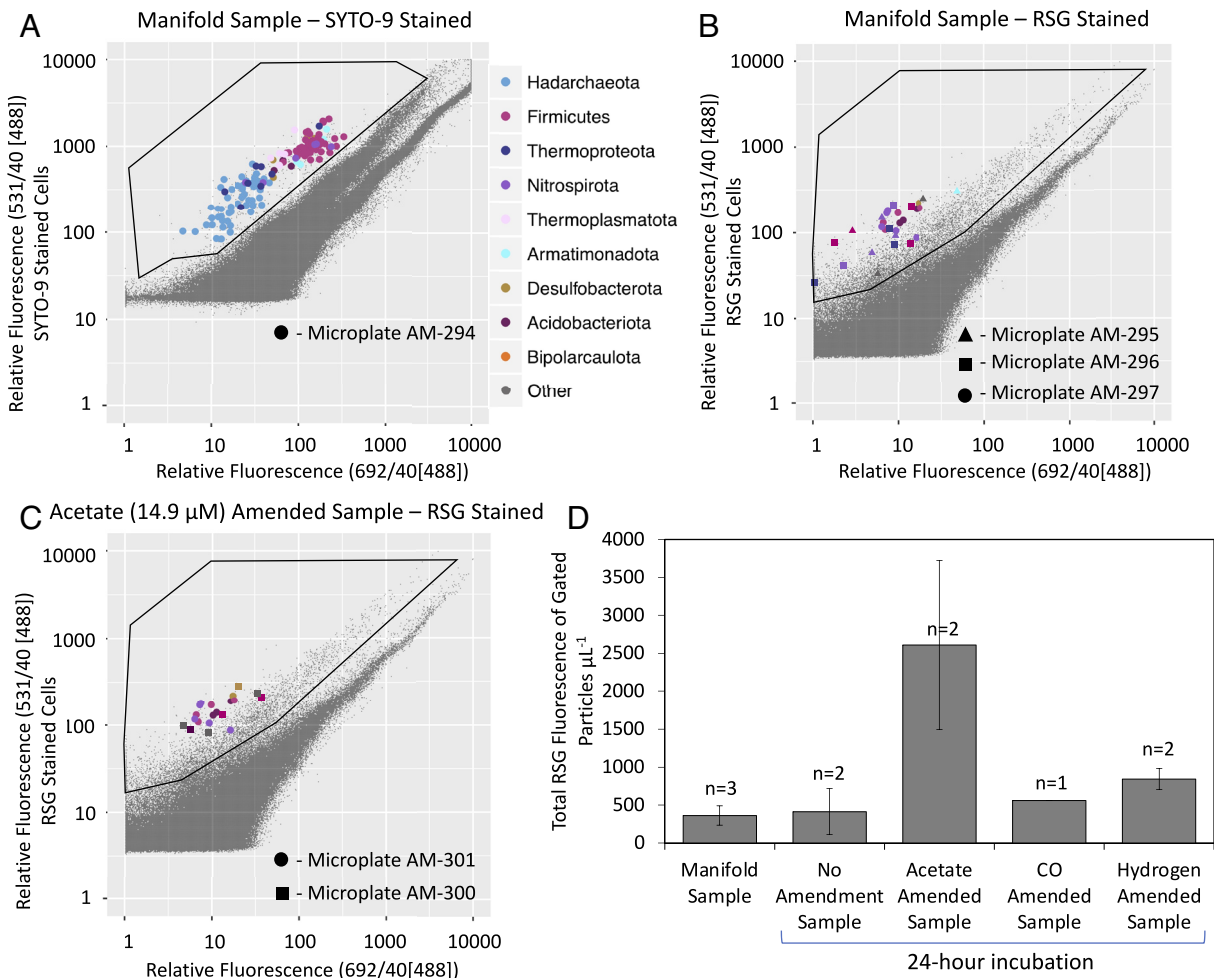

Fig. 2. Fluorescence intensity and taxonomic identity of cells from Inyo-BLM1 subsurface fluids as observed by flow cytometry. (A) Green fluorescence (y-axis) and red fluorescence (x-axis) of SYTO-9-stained particles recovered directly from the Inyo-BLM 1 manifold samples, from one FACS sort and one 384-well plate of sequencing (microplate AM-294), where green is fluorescence detected with 40 nm bandpass centered by 531 nm wavelength when excited with 488 nm light, and red is fluorescence detected with 40 nm bandpass centered by 692 nm wavelength when excited with 488 nm light. (B) Green fluorescence and red fluorescence from RSG-stained particles recovered directly from Inyo-BLM 1 manifold samples with similar detector settings as described for (A). This figure was constructed with data from three separate plates sorted from one sample (microplates AM-295, AM-296, and AM-297). (C) Green fluorescence and red fluorescence from RSG-stained particles recovered from Inyo-BLM 1 manifold fluids incubated at 65 °C under anoxic conditions with added acetate at 14.9 μM ("amended sample"). This figure was constructed with data from two separate plates sorted from one sample (microplates AM-300 and AM-301). For all three samples depicted in (A–C), particles with sequenced SAGs are highlighted in colored dots. The top nine phyla are colored with large dots, with all other phyla pooled and depicted as "Other." The smaller gray points indicate particles that also passed through the detectors but were not sorted into the 384-well gate for sequencing and analysis, including "background" noise and other unsorted cell-like particles. Other samples not included in the flow cytograms shown here (incubated with no amendment, CO, and H2) are plotted in *SI Appendix,* Fig. S8 and flow cytograms plotting green fluorescence (y-axis) versus side scatter (x-axis) are depicted in *SI Appendix,* Fig. S7. (D) Total RSG fluorescence of gated particles that represent "cell-like" particles in manifold fluids and incubated fluids with different additions incubated at 65 °C for 24 h. Total fluorescence was calculated by summing the green fluorescence of each cell in a sample, normalized to volume. Number of samples analyzed per treatment is indicated by "n." For logistical reasons, we were unable to analyze enough replicates to determine statistical significance of this stimulation, as the number of samples analyzed per treatment varied between 1 and 3.

was also observed for aerobic respiration (17). Thus, we used stationary-phase cultures for calibrating RSG fluorescence and respiration activity rates (Fig. 1). Together, these calibrations confirmed the use of RSG fluorescence intensity as a proxy for cell-specific respiration rates of these anaerobic metabolisms.

Phylogenetically Diverse Sulfate-Reducing Bacteria Are Abundant in a Deep Fractured Carbonate Aquifer. To negate potential drilling- and casing-associated artifacts, all samples were collected from a gastight flowing manifold supplied by a submersible pump after flushing with >50 hole volumes. Cell counts determined by staining with SYTO-9 and flow cytometry were 770 cells mL^{-1} in a pristine manifold sample. Cell concentrations of samples stained with RSG were 465 cells mL^{-1} in one of the unamended control samples that was incubated for 24 h, and 933, 332, and 748 cells mL^{-1} in parallel samples amended with acetate (14.9 μM), CO (9 μM), and H$_2$ (8 μM), respectively. Following FACS and single-amplified genome (SAG) sequencing, 138 SYTO-9- and 119 RSG-stained cells could be grouped into 17 species clusters of two or more cells at 95% average nucleotide identity (ANI) (*SI Appendix*, Fig. S5). The most abundant of these species clusters were identified by the Genome Taxonomy Database Toolkit (GTDB-Tk) as *Ca.* D. audaxviator (cluster 1; 47 SAGs), an unidentified species in the order *Candidatus* Hadarchaeales (cluster 2; 24 SAGs), an unidentified species in the order *Thermodesulfovibrionales* (cluster 3; 11 SAGs), and an unidentified species in the phylum *Desulfobacterota* (cluster 4; 11 SAGs). The dominance of *Ca.* D. audaxviator in the Inyo-BLM 1 subsurface ecosystem was consistent with previous studies at Inyo-BLM 1 and other ultradeep subsurface habitats (10, 18, 21). Overall, *Ca.* D. audaxviator, which encompasses SAGs belonging to several clusters (clusters 1, 14, and 16, and several unclustered SAGs) represented 34% of all SYTO-9-stained cells (47 SAGs) and 30% of all RSG-stained cells (36 SAGs) and was abundant in both the unamended manifold sample and in amended samples (Fig. 2 and Dataset S1). *Ca.* Hadarchaeales, *Thermodesulfovibrionales*, and *Desulfobacterota* are also often abundant in other terrestrial deep subsurface ecosystems globally (21, 32). Generally, the community composition of the manifold sample determined with single-cell sequencing agreed with 16S rRNA gene amplicon data (*SI Appendix*, Fig. S6), including samples collected from Inyo-BLM 1 pumped water collected at various timepoints since the hole was first drilled in 2007 (26, 30). However, there were minor differences in community composition between these two approaches, likely due to the limited number of SAGs that could be analyzed (209 total cells).

Three of the four most abundant species clusters, *Ca.* D. audaxviator (cluster 1), *Thermodesulfovibrionales* (cluster 3), and *Desulfobacterota* (cluster 4) encoded key genes involved in sulfate reduction, including sulfate adenylyltransferase (*sat*), adenylylsulfate reductase (*aprAB*), and dissimilatory sulfite reductase (*dsrABC*) (Fig. 3). Descriptions of these genes are detailed in Dataset S3, and the taxonomy of each SAG is detailed in Dataset S1. Notably, *Ca.* D. audaxviator encodes acetyl-CoA synthetase (*acs*) and was enriched among RSG-stained cells incubated with acetate, suggesting the cells were able to utilize acetate as a carbon source and electron donor, likely coupled to sulfate reduction (Figs. 2 *B* and *D* and 4*D*). A putative H$_2$ uptake hydrogenase belonging to the [NiFe]-hydrogenase group 1a (33) was also found in *Ca.* D. audaxviator genomes. Both acetate and hydrogen supported growth of a pure culture of *Ca.* D. audaxviator in the laboratory (20).

Application of the RSG-Based Proxy to Measure Single-Cell Sulfate Reduction Rates. As expected for an oligotrophic environment, the average RSG fluorescence of cells from Inyo-BLM 1 groundwater above detection limit of the flow cytometer (described in *SI Appendix, SI Text*) was low (Fig. 2 and *SI Appendix*, Figs. S7 and S8). Electron donor stimulation experiments with Inyo-BLM 1 fluids raised concentrations of acetate from ambient (below detection limit, <5 μM) to 14.9 (±5.1) μM, of CO from below detection limit (<5 μM) to 9 μM, and of H$_2$ from 0.206 μM to 8 μM (geochemistry and cell abundance for all samples are described in Dataset S2). There was an increase in cumulative RSG fluorescence of the whole community following acetate amendment, indicating metabolism of this substrate (Fig. 2 *C* and *D*). This comparison was done by adding bulk fluorescence measurements of all cells in each sample normalized to volume. RSG fluorescence of Inyo-BLM 1 cells with added CO or H$_2$ did not increase, indicating that the amendments did not stimulate additional respiration during the 24-h incubation on a bulk community scale.

We observed an overall decrease in RSG-derived sulfate reduction rates in the CO-amended incubation (Figs. 2*D* and 4*D*). This could be caused by the switch of some organisms from respiration to fermentative metabolisms that do not reduce RSG, or the toxicity of CO and/or formic acid, which decomposes into CO. Exceptions to this overall trend were *Thermoproteota* cells (clusters 8, 9, and 12) that each exhibited increased RSG fluorescence when CO was added (Fig. 4*D*), indicating that CO stimulated the respiration of these three species, which belong to three different taxonomic orders. This result points to an advantage of this single cell-resolved analysis: while the bulk measurements showed a potential inhibition by CO, we could still identify three taxa whose respiration was stimulated by CO addition. The addition of H$_2$ did not measurably inhibit or stimulate respiration in any species, which was surprising, given genomic predictions (18) and the ability of pure cultures of *Ca.* D. audaxviator to oxidize H$_2$ and the prevalence of hydrogenotrophy among known sulfate-reducing bacteria. Alternatively, the lack of H$_2$ stimulation could have been due to the adaptions of these lineages to low concentrations of H$_2$, or we may not have added a high enough concentration of H$_2$ to stimulate respiration.

Previous modeling studies of subsurface environments that take into account total numbers of cells when normalizing bulk rates have assumed that all cells of sulfate-reducing bacteria are equally active (34, 35). Our work shows that rates of sulfate reduction varied widely from cell to cell and species to species (Fig. 4 *A* and *D*). Although we did not have a sufficient number of SAGs to test the statistical significance of these differences, the variability in cell-specific rates implies that bulk rates cannot be accurately extrapolated to individual cells. This further underscores the importance of resolving species-specific activity rates when evaluating the physiological state of cells, especially considering that less abundant microbes can have a disproportionately large ecological impact (16, 17, 36). We also calculated the average sulfate reduction rate for cells from different taxa in the incubations, and this revealed the complexity in the response of different groups to different conditions (Fig. 4*D*). Overall, *Ca.* D. audaxviator (cluster 1) cells exhibited the highest cell-specific respiration rates in samples amended with acetate, while cells from the phylum *Desulfobacterota* (cluster 4 and cluster 15) exhibited high cell-specific respiration rates in the manifold sample (cluster 4 only) and in samples incubated with no amendment, acetate amendment, and H$_2$ amendment (cluster 4 and cluster 15) (Fig. 4*D*). *Thermodesulfovibrionales* cells (cluster 2 and cluster 5) either had low cell-specific respiration rates in all samples except the CO amendment (cluster 2) or were highly active in the manifold sample but were not recovered from electron donor amendments (cluster 5). Overall, these results indicate that the numerical abundance of various microbial taxa in the subsurface environment accessed through Inyo-BLM 1 does not always
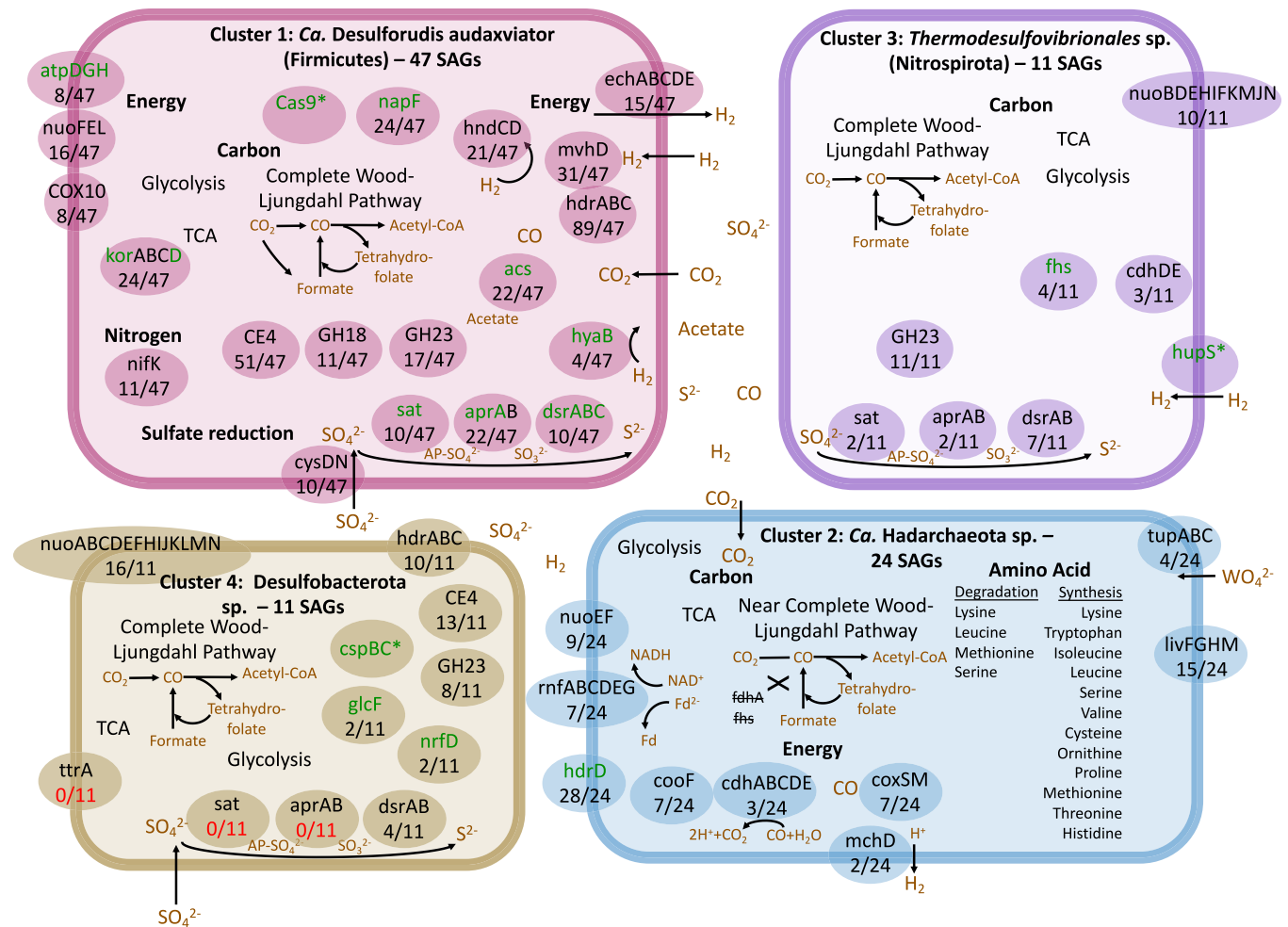
Fig. 3. Putative metabolic capabilities of the four most abundant SAG species clusters in the Inyo-BLM 1 samples—Firmicutes (cluster 1 which can be further classified to *Ca.* Desulforudis audaxviator), *Ca.* Hadarchaeota (cluster 2), Nitrospirota (cluster 3 which can be further classified to *Thermodesulfovibrionales*), and Desulfobacterota (cluster 4)—focusing on carbon cycling and energy sources. Genes in green text were present in transcriptome data (Dataset S3), whereas genes in black text were only present in the genomes. An * denotes genes that were classified from transcripts and mapped to SAG reads but were not annotated from SAG reads with DRAM. The number of copies of each gene out of the total number of SAGs for each species cluster (47, 24, 11, and 11 for *Ca.* D. audaxviator, *Ca.* Hadarchaeota, *Thermodesulfovibrionales*, and Desulfobacterota respectively) are shown below the gene names. All four species may use glycolysis and the TCA cycle for central carbon metabolism, while three species clusters (*Ca.* D. audaxviator, *Thermodesulfovibrionales*, and Desulfobacterota) encode complete Wood–Ljungdahl pathways, and some of the *Ca.* Hadarchaeota genomes only encode the carbonyl branch of the Wood–Ljungdahl pathway. Energy could be conserved in *Ca.* Desulforudis audaxviator and *Thermodesulfovibrionales* cells through dissimilatory sulfate reduction, as genomes in both species encode for key enzymes in the sulfate-reduction pathway (key genes include *sat*: sulfate adenylyltransferase, *dsrAB*: dissimilatory sulfite reductase, and *aprAB*: adenylylsulfate reductase). Desulfobacterota cells also encode *dsrAB*. Energy could be conserved in *Ca.* Hadarchaeota from hydrogenic CO oxidation, alongside proton reduction using carbon monoxide dehydrogenase (*cooF*), carbon monoxide dehydrogenase (*codh*), ferredoxin oxidoreductase complex (*rnf*), and a [NiFe]-hydrogenase group 4G, which is capable of forming a respiratory complex that couples ferredoxin oxidation with proton reduction (33). A full list of genes outlined in this figure with more detailed descriptions are in Dataset S4. Metabolic maps showing presence and absence of genes detailed in this figure for additional clusters can be found in SI Appendix, Fig. S13 (*Ca.* Desulforudis audaxviator), SI Appendix, Fig. S14 (*Ca.* Hadarchaeota), SI Appendix, Fig. S15 (Desulfobacterota), and SI Appendix, Fig. S16 (*Thermodesulfovibrionales*).

correlate with respiration activity, which was also shown in a prior study in coastal ocean water using similar tools (17).

Across all cells putatively capable of sulfate reduction based on our flow cytometry sorting, genome annotations, and ANI analysis of the SAGs (SI Appendix, SI Text and Materials and Methods), respiration rates varied between 0.14 and 26.9 fmol sulfate cell^{-1} h^{-1}, with no correlation between this process and estimated cell diameter (Fig. 4A and Dataset S1). This large range of sulfate reduction rates assigned to single cells indicates that cells contribute to elemental cycling at different orders of magnitude, and our RSG-based analyses offer a more detailed and potentially more accurate assessment of respiration rate differences between taxa and within taxa across different conditions (Fig. 1A). We then combined these single-cell rate data with counts of cells with the genetic potential for sulfate reduction

(SI Appendix, SI Text and Materials and Methods). This resulted in volume-specific sulfate reduction rate estimates of 1,377 (±254), 1,789 (±793), 1,068 (±165), 314 (±78), and 763 (±175) pmol sulfate L^{-1} d^{-1} in the manifold sample, the incubated unamended sample, the acetate-amended, the CO-amended, and the H$_2$-amended samples, respectively (Fig. 4B). In comparison, rates of bulk sulfate reduction determined by the ^{35}SO$_4^{2-}$ radiotracer ranged from 25 to 383 pmol sulfate L^{-1} d^1 (Fig. 4B), i.e., were slightly lower than RSG-based estimates. The discrepancy between radiotracer- and RSG-based rate estimates could be due to the radiotracer approach being a net rate measurement influenced by multiple ^{35}S cycling processes (37), while the RSG approach is a gross measurement of oxidoreductase activity. Additionally, radiotracer-based rates were at the limit of detection for the method and required 4 wk of incubation, during
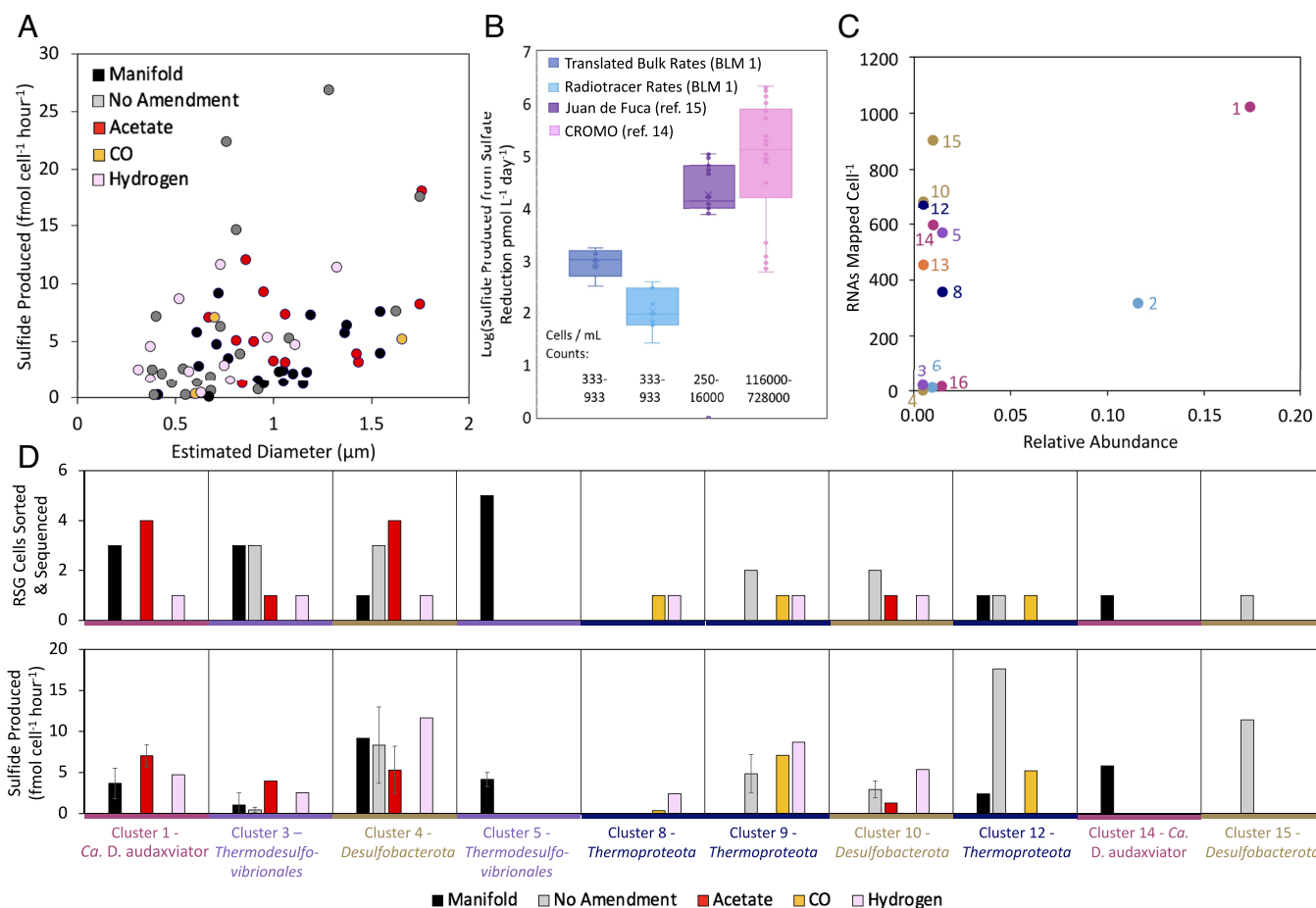
Fig. 4. Evidence for metabolic activity, active cells, and sulfate reducers in low-biomass Inyo-BLM 1 subsurface fluids. (*A*) Inferred rates of sulfate reduction by individual single cells of known taxonomy in Inyo-BLM 1 fluids calculated from the RSG-fluorescence calibration (Fig. 1*A*) versus estimated cell diameter inferred from forward scatter versus size-calibrated beads (methods for calculation described in *SI Appendix, SI Text* from ref. 17). Each cell either encoded for key genes involved in sulfate reduction in the SAG (*dsrAB* and *aprAB*) or was closely related (≥95% ANI) to another SAG within this study that encoded the key genes. SAG source indicated with symbol shapes and taxonomy indicated with symbol colors per legend. Per-cell sulfate reduction rates ranged from 0.1 to 27 fmol cell^{-1} h^{-1}, with highest per-cell rates observed for *Desulfobacterota*, *Thermoproteota*, and Firmicutes cells and lowest rates for *Nitrospirota* (*Thermodesulfovibrionales*) cells. Estimated cell diameters ranged from 0.4 to 1.8 μm. (*B*) Comparison of bulk sulfate reduction rates in Inyo-BLM 1 samples measured with two different approaches in this study—RSG-based [Translated Bulk Rates (BLM 1)] and $^{35}SO_4^{2-}$ radiotracer incubations [Radiotracer Rates (BLM 1)]—compared to radiotracer incubation-based measurements from other subsurface environments including the CROMO serpentinizing subsurface fluids (14); and subsurface oceanic crustal fluids from the Juan de Fuca Ridge flank (15). Translated Bulk Rate (RSG-based) estimates were calculated from cell-specific rates of sulfate reduction (from *A*) multiplied by the number of cells identified as sulfate-reducing bacteria per mL and normalized to volume run through the flow cytometer used to sort cells for sequencing. Values listed in Dataset S6. (*C*) Average 16S rRNA transcript quantities per cell and average relative abundance of cells within different 95% ANI species clusters from the manifold sample stained with RSG. The colors of the dots, in addition to being labeled according to the cluster #, follow the same color pattern as Figs. 2 and 3. (*D*) Average rates of sulfide production per cell for different sulfate reduction-capable SAG 95% ANI clusters (1, 3, 4, 5, 8, 9, 10, 12, 14, 15) across RSG-stained samples.

which electron donors or other resources may have become limiting, and the composition of microbial communities may have shifted. By contrast, the RSG incubations took only 30 min, substantially reducing the risk of major changes in chemical and biological properties of the samples. However, it is important to keep in mind that the RSG approach may overestimate sulfate reduction because the reduction of RSG may not be fully coupled to sulfate reduction in the analyzed cells. This is due to the uncertainties in the specific electron donors used, or potentially other alternative pathways used by each species that may trigger electron transfer to RSG. For example, the use of different electron donors including hydrogen or formate in *Ca.* D. audaxviator cells (18, 20) may have an unknown effect on RSG fluorescence based on the different fates of electrons. Interestingly, the rates measured with our RSG approach are higher than previously measured sulfate reduction rates that were normalized to cell number (31). These higher cell-specific rates over bulk rates make sense in light of the fact that bulk rates take into account both active and inactive cells, which could underestimate the activity of the most active cells in situ. This further highlights the diverse cell-specific rates made possible by this RSG approach and the importance of single-cell rate measurements. Nevertheless, both the RSG-based and radiotracer-based estimates indicate that despite relatively high sulfate concentrations (1.75 mM, Dataset S2), rates of sulfate reduction in the Inyo-BLM 1 system (25 to 383 pmol sulfate L^{-1} d^1) are lower than in other, previously studied, low-biomass deep biosphere systems, such as the Coast Range Ophiolite Microbial Observatory (600 to 2,047,700 pmol sulfate L^{-1} d^1) (14) and subsurface crustal fluids of the Juan de Fuca ridge flank (8,000 to 109,000 pmol sulfate L^{-1} d^1) (15).

Species-Specific Gene Expression by Subsurface Microbiota. To further tie RSG fluorescence to specific species and metabolisms, we used all Inyo-BLM 1 SAGs as a reference database for the taxonomic and functional annotation of a metatranscriptome

obtained from the Inyo-BLM 1 manifold sample (Dataset S4). Remarkably, metatranscriptome reads were recruited only to 196 out of a total of 297,564 protein-encoding genes. Of these 196 genes, 107 belonged to *Ca.* D. audaxviator. *Ca.* D. audaxviator also recruited the greatest number of rRNA reads (1,022 reads normalized to total cell number). These results provide further evidence that this species is abundant and active in this low-energy, deep subsurface environment (Fig. 4*C*). The detected *Ca.* D. audaxviator transcripts included *sat, aprA,* and *dsrABC,* which are subunits of key enzyme complexes involved in sulfate reduction, and *acsC* and *hyaB,* which are involved in the use of acetate and hydrogen as electron donors (Fig. 3 and Dataset S4). We also detected *Ca.* D. audaxviator transcripts of ATP synthase, which is consistent with chemiosmotic ATP production (Figs. 3 and 4*C* and Dataset S3). Cells of *Desulfobacterota*, particularly cluster 15, also exhibited high transcript counts (903 transcripts per cell), consistent with the relatively high respiration activity of this order as shown by high RSG fluorescence. However, none of these transcripts mapped to genes directly involved in sulfate reduction or any other catabolic pathway (Fig. 4*C*).

It is notable that 16S rRNAs, which is sometimes used as a general metabolic activity proxy (38), varied between 1 and 1,000 among genera (Fig. 4*C*). This range was similar to prior reports from seawater (17, 39, 40), although the average value was lower. We speculate that this overall low level of gene expression, and especially the very narrow spectrum of expressed genes, may represent an adaptation to living in an extremely oligotrophic environment, where cells minimize their transcription to conserve energy. Consistent with this hypothesis, as has been shown in other continental deep subsurface sites (41), most transcripts were related to energy metabolism, such as *dsrAB* or *aprAB*.

Unexpected Absence of Subsurface Methanogenesis. Intriguingly, no evidence for methanogenesis, methanotrophy, or alkanotrophy [oxidation of short-chain alkanes; (42)] was detected in samples from Inyo-BLM 1 either by taxonomic assignment of SAGs to canonical methanogens, annotation of methanogenic, methanotrophic, or alkanotrophic pathways in SAGs, or through bulk radiotracer methanogenesis measurements (Fig. 3), despite other studies of subsurface environments demonstrating the co-occurrence of sulfate reducers and methanogens (21, 43) and the presence of methane in these subsurface fluids measured at 151.5 μM in this study (Dataset S2). Methane was also previously observed at concentrations of up to 100 μM in previous years at this site (44). Additionally, attempts to measure bulk rates of hydrogenotrophic methanogenesis with ^{14}C-labeled dissolved inorganic carbon yielded values that were indistinguishable from formaldehyde-killed controls. This result may be time-dependent, however, since earlier pumped sampling intervals at Inyo-BLM 1 (in 2007 and 2011) did reveal much higher proportions of *Methanobacterium* and *Methanothermobacter* spp. in 16S rRNA gene libraries [28.6 and 52.7% of prokaryotes], than noted here (30). In these 2021 samples, the most abundant archaea, cluster 2 and cluster 6, belonged to the phylum *Ca.* Hadarchaeota and the order *Ca.* Hadarchaeales (Dataset S1 and *SI Appendix,* Fig. S5). Members of this phylum were first reported from the same ultradeep mine in South Africa, Driefontein, where *Ca.* Desulforudis audaxviator was initially detected (21, 45) and have been shown to encode one or two methyl-coenzyme M reductase (*mcr*) gene clusters that may function in alkanotrophy (46). However, in the present study the SAGs from cluster 2 and cluster 6 only encoded distant homologs of a single subunit

of *mcr, mcrB* (*SI Appendix,* Fig. S9), clustered separately from known methanogenic lineages (*SI Appendix,* Fig. S10), and lacked other *mcr* genes and other key genes for alkanotrophy. While the estimated genome completeness for *Ca.* Hadarchaeota SAGs ranged from 4 to 78%, our confidence for the absence of these pathways is high, due to the large number of *Ca.* Hadarchaeota SAGs sequenced. Future studies could examine the source of the methane that is observed in these well waters [Dataset S2, (44)], or directly assess anaerobic methanotrophy.

The abundant *Ca.* Hadarchaeota cells in Inyo-BLM 1 could potentially use carbon monoxide to fuel anaerobic CO oxidation via carbon monoxide dehydrogenase (*cdhABCDE*) using the "ferredoxin-like" electron carrier (*cooF*) (47) and an *ech* complex ([NiFe]-hydrogenase group 4G) that couples ferredoxin oxidation with proton reduction (33). The *Ca.* Hadarchaeota cells could fix carbon using the acetyl-CoA synthase/carbon monoxide dehydrogenase (*acs/codh*), and pyruvate ferredoxin oxidoreductase (*porABDG*). This basic metabolism has been previously described as a possible metabolism for other *Ca.* Hadarchaeota (32). CO was below method detection limits in Inyo-BLM 1 aquifer fluids (<5 μM, Dataset S2) but is common in environments influenced by hydrothermal activity and has been detected in other subsurface habitats where *Ca.* Hadarchaeota have been detected (21). CO could be produced by the thermal decomposition of organic matter, or as a side product of some anaerobes (48, 49). After sulfate reduction, the CO oxidation reaction has the greatest free energy flux among modeled anaerobic metabolisms in similar deep continental subsurface environments (9, 21). However, there was little evidence of respiration activity of *Ca.* Hadarchaeota in Inyo-BLM 1, aside from two cells present in the hydrogen-amended sample that were relatively low in RSG fluorescence (*SI Appendix,* Fig. S7 *I* and *J*). *Ca.* Hadarchaeota cells were not recovered from the CO-amended samples and very few mRNA or rRNA reads mapped to *Ca.* Hadarchaeota SAGs (Fig. 4*C* and Dataset S4).

Concluding Remarks

This study demonstrates the ability to make single-cell specific measurements of anaerobic respiration in ultralow biomass and low-energy ecosystems using flow cytometry integrated with single-cell genomics. Bulk rates of sulfate reduction derived from this single-cell method agreed well with a traditional radiotracer technique. The benefits of the reported approach include superior sensitivity, small sample volume requirements (1 mL is sufficient), short incubation times (30 min), single-cell resolution, and the direct linking of respiration measurements to the genome sequences of analyzed cells. We found that abundant *Ca.* Desulforudis audaxviator cells respire sulfate in situ, with both acetate and H_2 as electron donors, and likely contribute to a large proportion of elemental cycling and could be responsible for a majority of primary production. We also showed that less abundant members of the *Desulfobacterota* also had high specific sulfate reduction rates (Fig. 5), decoupling respiration rates from abundance of species. Unexpectedly, the study failed to find conclusive evidence for the presence and activity of methanogenic archaea, which differs from samples collected at Inyo-BLM 1 a decade earlier and other deep subsurface environments where sulfate reducers and hydrogenotrophic methanogens coexist. While this study focused on a deep subsurface habitat, this cell-specific method may be applicable for constraining anaerobic respiration rates of microbial cells, and in resolving the role of essential microbial taxa in a variety of anoxic environments.
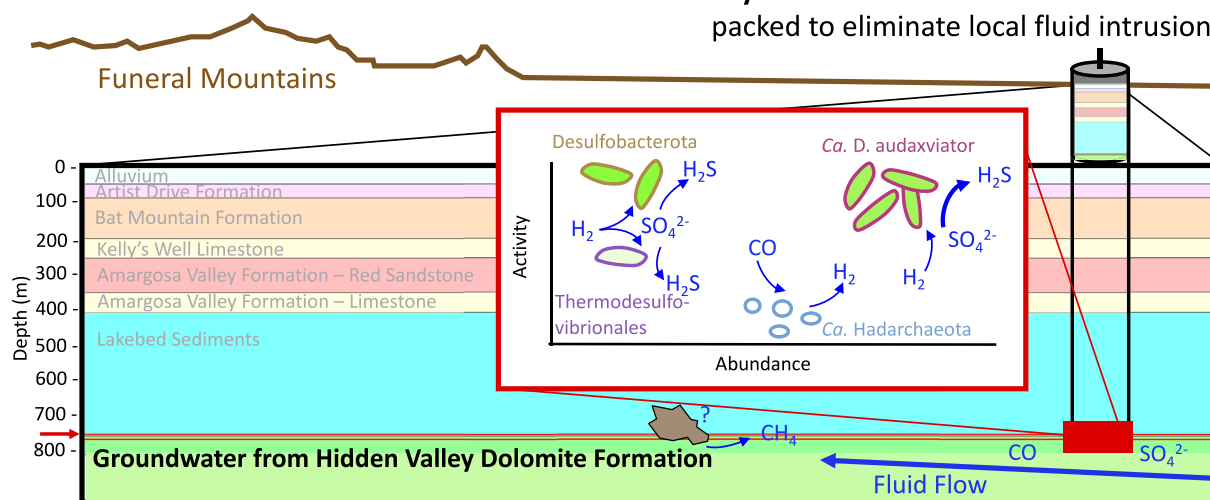
Fig. 5. Schematic summarizing the respiration activity, general relative abundance, and contributions of the dominant species in the subsurface Inyo BLM-1 ecosystem which was sampled via a well that was cased and packed to prevent localized fluid intrusion. *Ca.* D. audaxviator cells are the most abundant cells and one of the most active species, and exhibit evidence for active sulfate reduction activity, with highly active *Desulfobacterota* and active *Thermodesulfovibrionales* also capable of sulfate reduction. However, these other lineages are present in smaller numbers and exhibit lower levels of respiration. This subsurface system also hosts largely inactive *Ca.* Hadarchaeota cells, which are likely either not suited for the particular location in the aquifer that was sampled, or are dormant, waiting for substrate to become available. Image not to scale. Surface-land interface taken from Funeral Mountains Geologic Map (978-1-4113-3313-0) and geologic units from Mullin et al. (44). Fluid flow hypothesis from Merino et al. (26). Schematic not to scale.

Materials and Methods

Calibration of RSG Fluorescence against Anaerobic Respiration Using Microbial Cultures. The approach for calibrating RSG fluorescence as a proxy for anaerobic respiration followed the same concept recently described for aerobes (17), with methods fully described in *SI Appendix, SI Text*. For sulfate reduction, we tested isolates of *Archaeoglobus fulgidus* (DSM 4304) and *Desulfovibrio salexigens* (DSM 2638) from the German Collection of Microorganisms and Cell Cultures (DSMZ; Braunschweig, Germany) as well as an enrichment of *Desulforamulus putei* obtained from the Inyo-BLM 1 sampling site. These cultures were grown in recommended media at varying temperatures and nutrient conditions (Fig. 1 and Dataset S5). Sulfide production mediated by these cultures was measured using the Cord-Ruwisch method (50). To calculate rates of sulfate reduction/sulfide production per cell, cell abundance was determined by flow cytometry in subsamples of the culture material taken at the same time as sulfide measurements were made, as described below and as depicted in *SI Appendix*, Fig. S12. For analysis of methanogens, we investigated an isolate of *Methanosarcina barkeri* (DSM 2948) obtained from DSMZ and an isolate of thermophilic *Methanocaldococcus jannaschii* obtained from James Holden's laboratory, both grown according to DSMZ media conditions. An enrichment of *Methanobacterium* from the Inyo BLM-1 sample site was also used in this analysis. To quantify methanogen metabolic activity, methane (CH_4) production was measured by injecting 1 mL of headspace gas into an SRI 310C gas chromatograph. After the cultures reached stationary phase, 0.5 mL subsamples were obtained for each culture experiment, stained with 0.5 µL of the RSG stock solution (1 mM), and preserved for downstream FACS analysis on the ZE5 Cell Analyzer flow cytometer within 1 mo.

Our culture experiments yielded positive relationships between RSG fluorescence and the rate of production of sulfide by phylogenetically distinct sulfate-reducing microbes ($R^2 = 0.95$, Eq. **1**) and the rate of methane produced from both acetoclastic and hydrogenotrophic methanogenesis ($R^2 = 0.66$, Eq. **2**) according to these equations:

$$\text{fmol sulfide per cell per hour} = 0.9701 * \text{fluorescence}^{1.6816}, \quad [\mathbf{1}]$$

where "fmol sulfide per cell per hour" is the cell-specific respiration estimate of sulfide production from sulfate reduction, obtained by dividing bulk rates of sulfate reduction by the number of cells, and "fluorescence" is the mean of the normalized RSG fluorescence per cell in the culture, calculated to account for the difference between flow cytometry instruments. The numerical terms reflect the exponential relationship between sulfide production and RSG fluorescence. This equation is also depicted in Fig. 1*A*.

$$\text{amol methane per cell per hour} = 1.5854 * \text{fluorescence}^{1.7811}, \quad [\mathbf{2}]$$

where "amol methane per cell per hour" is the cell-specific estimate of methane production, obtained by dividing bulk rates of methanogenesis by the number of cells and "fluorescence" is the mean of the normalized RSG fluorescence per cell in the culture. The numerical terms reflect the exponential relationship between methane production and RSG fluorescence. This equation is also depicted in Fig. 1*B*. The positive relationships for both physiologies indicated that RSG responds to electron transfer from electron carriers for anaerobic metabolisms.

Description of Sample Site and Sample Collection. To demonstrate the utility of this respiration rate proxy approach, we applied RSG in the field to low-biomass, anoxic paleometeoric groundwater collected in April 2021 from the Inyo-BLM 1 well in the Amargosa Valley near Death Valley National Park. This well's design enables direct sampling of the named Lower Carbonate Aquifer in the discharge zone of the DVRFS (25, 27). The well uses an unscreened casing, hydrologically isolating shallower perched aquifers and other rock types, to access an inferred fracture zone in carbonate rock (primarily Paleozoic dolomite) from below the casing terminus at >750 mbls (Fig. 5). Prior to sampling, the hole was purged with many volumes of fracture water to minimize casing and drilling impacts and access an otherwise inaccessible pristine deep aquifer community, ultimately subsampled at surface through a custom manifold. Further description of the sampling borehole location and the formations through which the fluids are accessed are described in *SI Appendix, SI Text*.

Sampling and Incubation Set-Up. Stimulation experiments were performed on pumped Inyo-BLM 1 samples with added acetate, CO, and H_2 in 2 L glass bottles as described in *SI Appendix, SI Text*. Subsamples for geochemistry, FACS, analysis of bulk radioisotope respiration rate analyses, and single-cell genomics were taken from a freshly pumped sample, taken directly from the sampling manifold without further manipulations (referred to as "manifold" sample). Single-cell genomics samples consisted of an aliquot of cells stained either with SYTO-9 or RSG for activity assay measurements. Additional RSG-stained samples were taken from incubated amendment samples. All sample manipulations were conducted under anoxic conditions, which was maintained in collection bottles by overflowing the sample vessel with three bottle volumes of well water, as described in *SI Appendix, SI Text*. Metatranscriptome samples from unamended and amended samples were taken by filtering the remaining fluids through a 0.2 µm filter. Samples for measurements of gas concentrations (CO, H_2) and organic acids were collected and concentrations measured as described in *SI Appendix, SI Text*.

Single-Cell Fluorescence-Based Sorting, Genome Amplification, and Sequencing. FACS analyses for single-cell fluorescence measurements and cell size analysis were conducted on RSG-labeled and SYTO-9-labeled cells from amended and unamended samples using a BD InFlux Mariner flow cytometer equipped with a small particle detector according to previously published protocols (17, 51), with normalization as described in *SI Appendix, SI Text*. Flow cytometry standard data files are available in the FlowRepository public database under Repository ID FR-FCM-Z78B. Single-cell genome amplification, sequencing, and analysis followed previously described methods (17). FastANI was used to perform a pairwise ANI calculation (52) on all SAGs from all samples to cluster samples into lineages for analysis. Taxonomic assignments of SAGs and of metatranscriptomic reads (as detailed below) were obtained with GTDB-Tk v1.4.1 (53). For *Ca.* Hadarchaeota SAGs, further work looking at their placement within a phylogenetic tree and constructing a tree of *mcrB* genes was carried out using PhyloPhlAn v3.0.2 (54). All single amplified genome data are available under National Center for Biotechnology Information (NCBI) BioProject ID PRJNA853307.

Single-Cell RSG-Derived Rate Measurement Calculations. Any differences in day-to-day measurement drift due to the flow cytometer detectors were accounted for through concurrent analysis of estimated cell size and fluorescence standard kit beads as described in *SI Appendix, SI Text*. Using the calibration curves (i.e., Eqs. **1** and **2**) for fluorescence value transformed to a respiration rate (as detailed in the results section; Fig. 1), individual cell-specific respiration rates were calculated for all cells capable of sulfate reduction. This capability was determined through analysis for key genes involved in sulfate reduction as fully described in *SI Appendix, SI Text*.

Bulk Nucleic Acids Extraction, Amplicon and Metatranscriptomic Sequencing, and Analysis. Bulk DNA and RNA were extracted from filters from manifold and amended incubation samples. Analysis of 16S rRNA gene presence in bulk DNA extracts was conducted on a manifold sample taken at the same time as SAG samples and is fully described in *SI Appendix, SI Text*. RNA was extracted and metatranscriptomes analyzed according to methods described in *SI Appendix, SI Text*. Only transcripts which mapped onto SAGs from the same samples were considered to omit contamination. Transcript abundance on a per-cell basis was calculated for each sample and lineage separately as described in *SI Appendix, SI Text*. All metatranscriptome data are available under NCBI BioProject ID PRJNA1083713.

Bulk Radiotracer Sulfate Reduction and Methanogenesis Activity Measurement Sampling. Subsamples (30 mL each) were collected under anaerobic conditions from manifold fluids, incubated with amendments (where appropriate), and shipped under ambient conditions to collaborators at UCLA for radiotracer incubations. A ^{35}S-sulfate tracer was used in 28-d incubations to measure sulfate reduction activities, and a ^{14}C-bicarbonate tracer was used in 28-d incubations to measure methanogenesis activities. Full methods and rate calculations are described in *SI Appendix, SI Text*.

Data, Materials, and Software Availability. Single-cell genome and metatranscriptome data have been deposited in NCBI [BioProject nos. PRJNA853307 (55); PRJNA1083713 (56)], and flow cytometry data have been deposited in FlowRepository [dataset identifier FR-FCM-Z78B (57)].

Author affiliations: [a]Bigelow Laboratory for Ocean Sciences, East Boothbay, ME 04544; [b]Division of Hydrologic Sciences, Desert Research Institute, Las Vegas, NV 89119; [c]School of Life Sciences, University of Nevada Las Vegas, Las Vegas, NV 89154; [d]Department of Geology, Oberlin College, Oberlin, OH 44074; [e]Department of Marine and Environmental Sciences, Northeastern University, Boston, MA 02115; [f]Department of Earth, Planetary, and Space Sciences, University of California Los Angeles, Los Angeles, CA 90095; [g]Department of Microbiology, Southern Illinois University Carbondale, Carbondale, IL 62901; [h]School of the Earth, Ocean and Environment, University of South Carolina, Columbia, SC 29208; and [i]Department of Atmospheric and Oceanic Sciences, University of California Los Angeles, Los Angeles, CA 90095

1. Y. M. Bar-On, R. Phillips, R. Milo, The biomass distribution on Earth. *Proc. Natl. Acad. Sci. U.S.A.* **115**, 6506–6511 (2018).
2. H.-C. Flemming, S. Wuertz, Bacteria and archaea on Earth and their abundance in biofilms. *Nat. Rev. Microbiol.* **17**, 247–260 (2019).
3. C. Magnabosco *et al.*, The biomass and biodiversity of the continental subsurface. *Nat. Geosci.* **11**, 707–717 (2018).
4. T. M. Hoehler, B. B. Jørgensen, Microbial life under extreme energy limitation. *Nat. Rev. Microbiol.* **11**, 83–94 (2013).
5. J. R. Michalski *et al.*, The Martian subsurface as a potential window into the origin of life. *Nat. Geosci.* **11**, 21–26 (2017).
6. S. Vance *et al.*, Hydrothermal systems in small ocean planets. *Astrobiology* **7**, 987–1005 (2007).
7. B. M. Jakosky, E. L. Shock, The biological potential of Mars, the early Earth, and Europa. *J. Geophys. Res.* **103**, 19359–19364 (1998).
8. D. R. Lovley, F. H. Chapelle, Deep subsurface microbial processes. *Rev. Geophys.* **33**, 365–381 (1995).
9. C. Magnabosco *et al.*, A metagenomic window into carbon metabolism at 3 km depth in Precambrian continental crust. *ISME J.* **10**, 730–741 (2016).
10. M. C. Y. Lau *et al.*, An oligotrophic deep-subsurface community dependent on syntrophy is dominated by sulfur-driven autotrophic denitrifiers. *Proc. Natl. Acad. Sci. U.S.A.* **113**, E7927–E7936 (2016).
11. K. J. Edwards, K. Becker, F. Colwell, The deep, dark energy biosphere: Intraterrestrial life on Earth. *Annu. Rev. Earth Planet. Sci.* **40**, 551–568 (2012).
12. T. M. McCollum, J. P. Amend, A thermodynamic assessment of energy requirements for biomass synthesis by chemolithoautotrophic micro-organisms in oxic and anoxic environments. *Geobiology* **3**, 135–144 (2005).
13. E. Bell *et al.*, Active sulfur cycling in the terrestrial deep subsurface. *ISME J.* **14**, 1260–1272 (2020).
14. C. Glombitza *et al.*, Active microbial sulfate reduction in fluids of serpentinizing peridotites of the continental subsurface. *Commun. Earth Environ.* **2**, 84 (2021).
15. A. Robador *et al.*, Activity and phylogenetic diversity of sulfate-reducing microorganisms in low-temperature subsurface fluids within the upper oceanic crust. *Front. Microbiol.* **5**, 748 (2015).
16. N. Musat *et al.*, A single-cell view on the ecophysiology of anaerobic phototrophic bacteria. *Proc. Natl. Acad. Sci. U.S.A.* **105**, 17861–17866 (2008).
17. J. H. Munson-McGee *et al.*, Decoupling of respiration rates and abundance in marine prokaryoplankton. *Nature* **612**, 764–770 (2022).
18. D. Chivian *et al.*, Environmental genomics reveals a single-species ecosystem deep within Earth. *Science* **322**, 275–278 (2008).
19. E. D. Becraft *et al.*, Evolutionary stasis of a deep subsurface microbial lineage. *ISME J.* **15**, 2830–2842 (2021).
20. O. V. Karnachuk *et al.*, Domestication of previously uncultivated *Candidatus* Desulforudis audaxviator from a deep aquifer in Siberia sheds light on its physiology and evolution. *ISME J.* **13**, 1947–1959 (2019).
21. D. P. Moser *et al.*, *Desulfotomaculum* and *Methanobacterium* spp. dominate a 4- to 5-kilometer-deep fault. *Appl. Environ. Microbiol.* **71**, 8773–8783 (2005).
22. W. D. Orsi, V. P. Edgcomb, G. D. Christman, J. F. Biddle, Gene expression in the deep biosphere. *Nature* **499**, 205–208 (2013).
23. G. E. Fogg, O. Calvario-Martinez, Effects of bottle size in determinations of primary productivity by phytoplankton. *Hydrobiologia* **173**, 89–94 (1989).
24. M. G. Kalyuzhnaya, M. E. Lidstrom, L. Chistoserdova, Real-time detection of actively metabolizing microbes by redox sensing as applied to methylotroph populations in Lake Washington. *ISME J.* **2**, 696–706 (2008).
25. M. J. King, J. D. Bredehoft, "Death Valley springs geochemical investigation: Yucca Mountain Nuclear Repository, Inyo Country oversight-1998" in *Yucca Mountain Repository Oversight Program*, I. C. P. Department, Ed. (The HYDRODYNAMICS Group, 1999), p. 40.
26. N. Merino *et al.*, Subsurface microbial communities as a tool for characterizing regional-scale groundwater flow. *Sci. Total Environ.* **842**, 156768 (2022).
27. W. R. Belcher, M. S. Bedinger, J. T. Back, D. S. Sweetkind, Interbasin flow in the Great Basin with special reference to the southern Funeral Mountains and the source of Furnace Creek springs, Death Valley, California, U.S. *J. Hydrol.* **369**, 30–43 (2009).
28. M. C. Konopka *et al.*, Respiration response imaging for real-time detection of microbial function at the single-cell level. *Appl. Environ. Microbiol.* **77**, 67–72 (2011).
29. A. R. Rowe *et al.*, Tracking electron uptake from a cathode into *Shewanella* cells: Implications for energy aquisition from solid-substrate electron donors. *mBio* **9**, e02203-17 (2018).

30. J. D. Sackett, "Prokaryotic diversity and aqueous geochemistry of subsurface environments of the Death Valley regional flow system," PhD thesis, University of Nevada Las Vegas, Nevada (2018).

31. B. B. Jørgensen, A. J. Findlay, A. Pellerin, The biogeochemical sulfur cycle of marine sediments. *Front. Microbiol.* **10**, 849 (2019).

32. B. J. Baker *et al.*, Genomic inference of the metabolism of cosmopolitan subsurface Archaea, Hadesarchaea. *Nat. Microbiol.* **1**, 16002 (2016).

33. D. Søndergaard, C. N. S. Petersen, C. Greening, HydDB: A web tool for hydrogenase classification and analyses. *Sci. Rep.* **6**, 34212 (2017).

34. M. W. Bowles, J. M. Mogollón, S. Kasten, M. Zabel, K. Hinrichs, Global rates of marine sulfate reduction and implications for sub-sea-floor metabolic activities. *Science* **344**, 889–891 (2014).

35. J. A. Bradley *et al.*, Widespread energy limitation to life in global subseafloor sediments. *Sci. Adv.* **6**, eaba0697 (2020).

36. E. L. Fleming *et al.*, Insights into the fundamental physiology of the uncultured Fe-oxidizing bacterium *Leptothrix ochracea. Appl. Environ. Microbiol.* **84**, e02239-17 (2018).

37. T. Treude, L. J. Hamdan, S. Lemieux, A. W. Dale, S. Sommer, Rapid sulfur cycling in sediments from the Peruvian oxygen minimum zone featuring simultaneous sulfate reduction and sulfide oxidation. *Limnol. Oceanogr.* **66**, 2661–2671 (2021).

38. S. J. Blazewicz, R. L. Barnard, R. A. Daly, M. K. Firestone, Evaluating rRNA as an indicator of microbial activity in environmental communities: Limitations and uses. *ISME J.* **7**, 2061–2068 (2013).

39. M. A. Moran *et al.*, Sizing up metatranscriptomics. *ISME J.* **7**, 237–243 (2013).

40. K. Zwirgimaier, W. Ludwig, K.-H. Schleifer, Recognition of individual genes in a single bacterial cell by fluorescence *in situ* hybridization–RING-FISH. *Mol. Microbiol.* **51**, 89–96 (2004).

41. L. Purkamo *et al.*, Microbial co-occurence patterns in deep Precambrian bedrock fracture fluids. *Biogeosciences* **13**, 3091–3108 (2016).

42. O. N. Lemaire, T. Wagner, A structural view of alkyl-coenzyme M reductases, the first step of alkane anaerobic oxidation catalyzed by Archaea. *Biochemistry* **61**, 805–821 (2022).

43. A. W. Glossner *et al.*, Factors controlling the co-occurrence of microbial sulfate reduction and methanogenesis in coal bed reservoirs. *Int. J. Coal Geol.* **165**, 121–132 (2016).

44. S. W. Mullin *et al.*, Patterns of *in situ* mineral colonization by microorganisms in a ~60 °C deep continental subsurface aquifer. *Front. Microbiol.* **11**, 536535 (2020).

45. K. Takai, D. P. Moser, M. DeFlaun, T. C. Onstott, J. K. Fredrickson, Archaeal diversity in waters from deep South African gold mines. *Appl. Environ. Microbiol.* **67**, 5750–5760 (2001).

46. P. N. Evans *et al.*, An evolving view of methane metabolism in the Archaea. *Nat. Rev. Microbiol.* **17**, 219–232 (2019).

47. M. Diender, A. J. M. Stams, D. Z. Sousa, Pathways and bioenergetics of anaerobic carbon monoxide fermentation. *Front. Microbiol.* **6**, 1275 (2015).

48. T. V. Kochetkova *et al.*, Anaerobic transformation of carbon monoxide by microbial communities of Kamchatka hot springs. *Extremophiles* **15**, 319–325 (2011).

49. T. G. Sokolova *et al.*, Diversity and ecophysiological features of thermophilic carboxydotrophic anaerobes. *FEMS Microbiol. Ecol.* **68**, 131–141 (2009).

50. R. Cord-Ruwisch, A quick method for the determination of dissolved and precipitated sulfides in cultures of sulfate-reducing bacteria. *J. Microbiol. Methods* **4**, 33–36 (1985).

51. R. Stepanauskas *et al.*, Improved genome recovery and integrated cell-size analyses of individual uncultured microbial cells and viral particles. *Nat. Commun.* **8**, 84 (2017).

52. C. Jain, R. L. M. Rodriguez, A. M. Phillippy, K. T. Konstantinidis, S. Aluru, High throughput ANI analysis of 90K prokaryotic genomes reveals clear species boundaries. *Nat. Commun.* **9**, 1–8 (2018).

53. D. H. Parks *et al.*, GTDB: An ongoing census of bacterial and archaeal diversity through a phylogenetically consistent, rank normalized and complete genome-based taxonomy. *Nucleic Acids Res.* **50**, D785–D794 (2022).

54. F. Asnicar *et al.*, Precise phylogenetic analysis of microbial isolates and genomes from metagenomes using PhyloPhlAn 3.0. *Nat. Commun.* **11**, 2500 (2020).

55. M. Lindsay, Data from "Single cell genomes of multiple bacteria and archaea." NCBI. https://www.ncbi.nlm.nih.gov/bioproject?term=PRJNA853307. Deposited 27 June 2022.

56. M. Lindsay, Data from "Metatranscriptomes of samples containing bacteria and archaea found within a deep subsurface aquifer in the Death Valley Regional flow system." NCBI. https://www.ncbi.nlm.nih.gov/bioproject?term=PRJNA1083713. Deposited 4 March 2024.

57. M. Lindsay, Data from "Microbial genomes to phenomes: deep subsurface aquifer." FlowRepository. http://flowrepository.org/id/FR-FCM-Z78B. Deposited 4 March 2024.